Tectonophysics 627 (2014) 182–192

Contents lists available at ScienceDirect

Tectonophysics

journal homepage: www.elsevier.com/locate/tecto

Hypocentral parameter inversion for regions with poorly known velocity structures

Woohan Kim [a], Tae-Kyung Hong [b,*], Tae-Seob Kang [c]

[a] Gyeongsang National University, Department of Earth and Environmental Sciences and RINS, Jinju, Gyeongsangnam-do 660-701, South Korea
[b] Yonsei University, Department of Earth System Sciences, Shinchon-dong, 134, Seodaemun-gu, Seoul 120-749, South Korea
[c] Pukyong National University, Department of Earth Environmental Sciences, Daeyeon 3-dong, Nam-gu, Busan 608-737, South Korea

ARTICLE INFO

Article history:
Received 4 January 2013
Received in revised form 10 June 2013
Accepted 24 June 2013
Available online 4 July 2013

Keywords:
Hypocentral parameter inversion
Poorly known velocity structures
Algorithm
Best-fit velocity model

ABSTRACT

The determination of accurate hypocentral parameters is crucial in seismic monitoring, and is highly dependent on the accuracy of the implemented velocity model in conventional methods. A method to determine accurate hypocentral parameters based on an approximate velocity model is desirable. We introduce an iterative velocity updating scheme that can be readily combined with conventional hypocentral inversion methods. The algorithm searches for an optimum velocity model in a prescribed velocity range that minimizes the traveltime residuals. The hypocentral parameters are determined using the optimum velocity model. The proposed scheme reduces the dependence on a given velocity model in hypocentral inversion, providing reasonable hypocentral parameters based on an approximate velocity model. The feasibility and accuracy of the algorithm are tested with synthetic and field data. The scheme yields hypocentral parameters that are as accurate as those from full inversion methods but with approximately 70 times lower cost in terms of computational time. The proposed scheme can be readily implemented in any conventional method that is based on a fixed velocity model.

1. Introduction

Hypocentral parameters provide vital source information that includes the epicentral location (latitude, longitude), focal depth, and origin time. The determination of accurate hypocentral parameters is crucial in seismic monitoring. Standard location methods are based on Geiger's method (Geiger, 1912), which becomes practical with the advent of modern computers (Bolt, 1960; Flinn, 1965; Engdahl and Gunst, 1966). In addition, various hypocentral inversion methods have been introduced, including the joint hypocenter determination (JHD) (Douglas, 1967; Pujol, 1988), HYPO71 (Lee and Lahr, 1975; Lee, 1990), HYPOINVERSE (Klein, 1978, 2002), HYPOELLIPSE (Lahr, 1980, 1999), VELEST (Kissling et al., 1994), and HYPOSAT (Schweitzer, 1997, 2001). Hypocentral inversion methods are performed based on the assumption that the residuals between the theoretical and observed traveltimes are the minimums. Conventional methods implement fixed velocity models, and calculate theoretical traveltimes based on the velocity models (e.g., Asch et al., 1996; Delibasis et al., 1999; Gambino et al., 2004; Ito et al., 2012; Magistrale et al., 1989). Thus, the conventional methods based on fixed velocity models can yield correct hypocentral parameters only when accurate velocity models are implemented (e.g., Chiarabba and Frepoli, 1997; Hahm et al., 2007; Husen et al., 1999).

Hypocentral inversion methods determining both the hypocentral parameters and velocity structures simultaneously have been developed to avoid errors arising from implementation of incorrect velocity models, and were found to be useful for analyzing multiple events (e.g., Kissling et al., 1994; Pavlis and Booker, 1983; Thurber, 1985, 1992). In these methods, the seismic velocities in each layer are considered to be additional unknown parameters. However, such methods are not only expensive in terms of computation, but may also yield parameters and velocity structures that vary according to the initial velocity model implemented. Thus, to obtain accurate parameters, the initial velocity model may have to closely approximate the actual velocity structure. However, one- and two-dimensional (1-D and 2-D, respectively) velocity models have inherent limitations in representing actual three-dimensional (3-D) Earth structures.

A double-difference method based on differential traveltimes (hypoDD) was found to be useful for analyzing clustered events (Waldhauser and Ellsworth, 2000; Waldhauser, 2001). The method determines the relative locations of clustered events from traveltime differences among pairs of waveforms that are estimated precisely with the help of waveform cross-correlation. However, the initial hypocentral parameters in hypoDD are calculated by the conventional methods, and thus the hypocentral parameters depend on the velocity model implemented. In other words, the hypocentral parameters from hypoDD are inherently dependent on the reference velocity models. In addition, hypoDD can be applied only to clustered events, which limits its application (e.g., Lin et al., 2007; Prejean et al., 2004; Waldhauser and Schaff, 2008).

* Corresponding author. Tel.: +82 2 2123 2667.
E-mail addresses: wookim@gnu.ac.kr (W. Kim), tkhong@yonsei.ac.kr (T.-K. Hong), tskang@pknu.ac.kr (T.-S. Kang).

0040-1951/$ – see front matter © 2013 Elsevier B.V. All rights reserved.
http://dx.doi.org/10.1016/j.tecto.2013.06.024

Novel inversion methods are needed to allow for estimating accurate hypocentral parameters with little dependence on the given or initial velocity model. Such methods would be particularly useful for regions in which the velocity structures are poorly known. Kim et al. (2006) proposed a full inversion method based on a genetic algorithm, GA-MHYPO, which determines both a best-fitting velocity model and hypocentral parameters. Here, the best-fitting model is an optimum velocity model that yields the minimum traveltime residual in the hypocentral inversion. The GA-MHYPO yields hypocentral parameters with higher accuracy than conventional methods, and is rarely dependent on the initial velocity model (Hahm et al., 2007). However, GA-MHYPO suffers from high computational costs owing to iterative velocity refinement based on the genetic algorithm, which hinders prompt analysis in practical application (Hahm et al., 2007).

In this study, we introduce an accurate and computationally low-cost scheme to determine the hypocentral parameters based on an optimum 1-D velocity model yielding a minimum misfit error. The optimum velocity model is searched for iteratively by shifting an initial reference model within a prescribed range. The accuracy of the algorithm is then tested using synthetic data. Finally, we examine the applicability of the algorithm to conventional inversion methods.

2. Inversion scheme

2.1. Theory

The accuracy of inverted hypocentral parameters depends on the waveform quality, station distribution, velocity model, and accuracy of the inversion algorithm and two-point ray tracing. Thus, the accuracy of the velocity model is important for correct determination of hypocentral parameters. However, actual velocity structures are often poorly known, making use of an approximate 1-D velocity model. Such 1-D velocity models are designed so as to minimize the differences between observed and theoretical traveltimes by adjusting the number of layers, thicknesses of layers, velocities in each layer, and velocity contrasts across boundaries. Thus, the 1-D velocity models naturally incorporate errors into the hypocentral parameters. An algorithm is needed by which accurate hypocentral parameters can be determined using an approximate 1-D velocity model.

We propose an algorithm that searches for an optimum 1-D velocity model yielding minimum misfit errors for hypocentral inversions. All the model parameters such as the number, thicknesses, and velocities of layers are considered to be unknown. The optimum velocity model is determined by modifying the velocities in each layer of a given velocity model having a constant number of layers and constant thicknesses of layers. This approach is based on the idea that a velocity model with a proper average velocity and velocity gradient will produce synthetic traveltimes that are close to observed traveltimes with a sufficient level of accuracy. Here, the implemented average velocity may be close to that of the actual structure.

We first determine a semi-optimum 1-D P and S velocity model. We prepare a set of P velocity models that are shifted by constant velocities from the initial P velocity model:

$$\alpha_i^n = \alpha_i^0 + n\Delta\alpha, \quad (n = 0, 1, \cdots, N), \tag{1}$$

where $\Delta\alpha$ is a constant velocity interval, n is an integer varying from 0 to N, α_i^0 is the P velocity in the ith layer of the initial velocity model, and α_i^n is the P velocity in the ith layer of the nth velocity model prepared. The number of velocity models prepared is $N + 1$. That is, the nth P velocity model is designed by adding constant velocities of $n\Delta\alpha$ to the P velocity in each layer of the initial P velocity model. Here, the S velocity models are prepared subsequently from the P velocity model and a given V_P/V_S ratio. We set the V_P/V_S ratio to vary between 1.6 and 1.9 considering the typical V_P/V_S ratios in the crust.

The synthetic traveltimes of P and S phases are calculated for every velocity model, and the misfit error between the synthetic and observed traveltimes is estimated. Here, the misfit error, F, is assessed by

$$F = \frac{\sqrt{3\overline{\Delta t_p}^2 + \overline{\Delta t_s}^2}}{4}, \tag{2}$$

where $\overline{\Delta t_p}$ and $\overline{\Delta t_s}$ are traveltime differences (residuals) of P and S waves, respectively. The velocity model with the minimum misfit error is selected as the optimum velocity model. Here considering the relative certainty in the estimation of traveltimes, the traveltime errors of P waves are counted with a three-times-larger weight than those of S waves (Kim et al., 2006).

The traveltime differences of P and S waves ($\overline{\Delta t_p}, \overline{\Delta t_s}$) are calculated by

$$\overline{\Delta t_p}^2 = \frac{\sum_{k=1}^{n_p}\left(w_p^k \Delta t_p^k\right)^2}{\sum_k^{n_p}\left(w_p^k\right)^2}, \quad \overline{\Delta t_s}^2 = \frac{\sum_{k=1}^{n_s}\left(w_s^k \Delta t_s^k\right)^2}{\sum_k^{n_s}\left(w_s^k\right)^2}, \tag{3}$$

where n_p and n_s are the numbers of stations in which P and S arrival times are recorded, Δt_l^k is the traveltime residual of phase l at the kth station, and w_l^k is the weighting factor for phase l at the kth station.

We further refine the velocity model by searching the optimum vertical velocity gradient. A set of velocity models modified from the semi-optimum velocity model is prepared. The P velocity in the first layer is varied in a prescribed range. The P velocities in lower layers are calculated by

$$\alpha_i^{mod} = \alpha_i^{so} + \left(\alpha_1^{mod} - \alpha_1^{so}\right) \times \frac{\overline{\alpha} - \alpha_i^{so}}{\overline{\alpha} - \alpha_1^{so}}, \tag{4}$$

where α_i^{mod} is the modified P velocity for the ith layer, and α_i^{so} is the P velocity for the ith layer in the semi-optimum model. Parameter $\overline{\alpha}$ is the weighted average P velocity of the velocity model given by (Fäh et al., 2001)

$$\overline{\alpha} = \frac{\sum_{i=1}^{N} \alpha_i h_i}{\sum_{i=1}^{N} h_i}, \tag{5}$$

where α_i is the P velocity of the ith layer, h_i is the thickness of the ith layer, and N is the number of layers in the velocity model.

The misfit errors for the set of velocity models are estimated. A velocity model with the minimum misfit error is selected as an optimum velocity model for a given velocity interval ($\Delta\alpha$). This selected velocity model can be used as a new initial reference velocity model for further refinement of the velocity model, which can be achieved by iterative implementation with a smaller $\Delta\alpha$ in Eq. (1). The velocity-refinement procedure is repeated until a sufficiently small $\Delta\alpha$ is applied. The velocity model with the minimum misfit error for implementation of the smallest $\Delta\alpha$ is considered the final optimum velocity model.

2.2. Implementation of velocity model

The optimum P velocity model is determined by iterative refinement of the velocity model with consecutive implementation of a smaller $\Delta\alpha$ in Eq. (1). For model refinement, we prepare a set of $\Delta\alpha$ that is composed of (0.1 km/s, 0.01 km/s, ⋯, 10^{-m} km/s) where m is an integer. In practice, the integer m can be set considering the typical levels of errors in phase picking and hypocentral inversion. In this presentation, we consider the model refinement up to $m = 4$ which is a challenging level of accuracy.

In every refinement of velocity, we improve the accuracy of the velocities to higher places of decimals. For example, when we refine the velocity model with a $\Delta\alpha$ of 0.01 km/s, we improve the accuracy of the velocity to two decimal places. In this case, the optimum

velocity model to one decimal place is used as the reference velocity model in the determination of an optimum velocity model to two places of decimals. The optimum velocities to two decimal places are searched in ranges between −0.05 and 0.04 km/s with respect to the optimum velocities to one decimal place. Such consecutive refinement of velocity models with application of a smaller $\Delta\alpha$ allows us to reduce the computational time effectively.

Fig. 1 presents an example of the model refinement scheme for a velocity model with a weighted average velocity that is larger by 0.1785 km/s than the reference velocity model applied. In the first round of model refinement, an optimum velocity to one decimal place is searched between −0.6 and 0.6 km/s with respect to the reference velocity at $\Delta\alpha$ of 0.1 km/s. The velocity range to be searched in the first round of model refinement is determined considering the plausible velocities in the medium. In the example in Fig. 1, the optimum velocity with the minimum misfit error is found at the velocity shifted by 0.2 km/s. In the second round of velocity refinement which tunes the velocity to two decimal places, the velocity difference varies between −0.05 and 0.04 km/s with $\Delta\alpha$ of 0.01 km/s around the optimum velocity to one decimal place, i.e., 0.15–0.24 km/s. Here, the minimum misfit error is found at a velocity difference of 0.18 km/s.

In the third round of model refinement, the optimum velocity to three decimal places is found between 0.175 and 0.184 km/s with a velocity interval of 0.001 km/s. The optimum velocity to three decimal places is found at a velocity difference of 0.179 km/s (Fig. 1). The model refinement continues until the misfit error between the synthetic and observed traveltimes is less than the prescribed value. The hypocentral parameters converge with the number of model refinements. Considering the sampling rates of typical recording systems and the resolution of the inversion scheme, the hypocentral parameters are expected to converge within the fifth round of model refinement. Note that we search for the optimum velocity gradient in the first round of model refinement. The determination of the optimum velocity gradient can be omitted in further rounds of model refinement to higher places of decimals.

3. Velocity models and synthetic data

We apply the proposed algorithm to conventional methods, and test the accuracy of the inverted hypocentral parameters. We also check the dependency of the inverted hypocentral parameters on the implemented velocity models. Validation tests are conducted for both noise-free and noise-added synthetic data. The true velocity model is composed of nine layers with irregular intervals between boundaries (Table 1, Fig. 2(a)). The V_P/V_S ratio varies in each layer.

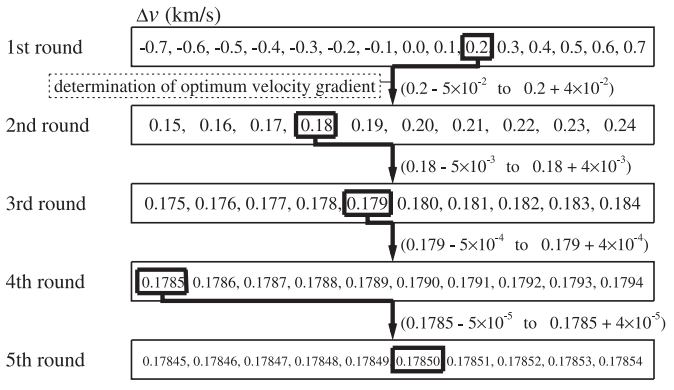

Fig. 1. The iterative velocity refinement scheme adopted in this study. The true velocity is higher than the initial velocity by 0.1785 km/s. A best-fit velocity is determined from the given data set, and an optimum velocity gradient is determined after the first round of velocity refinement. The velocity refinement is limited by the sampling rates of waveforms.

Two models with 11 layers (models A and B) are used as the reference velocity models in the inversions of hypocentral parameters (Table 2, Fig. 2(a)). The velocities in model A are set to be lower than those in the true model, while those in model B are set to be larger. In addition, the numbers of layers and depths to boundaries are set to be different between the true model and reference models. Furthermore, low-velocity layers are not included in the reference models, unlike the true velocity model. Thus, the 11-layered reference models neither resemble nor reflect the true model reasonably, which is a common situation encountered in the field.

We also prescribe a velocity range for the inversion method (e.g., GA-MHYPO), which searches for the best-fit velocity model within a given velocity range. The velocity range is designed to include all plausible velocities in the medium. In this study, we design the 1-D bounding *P* velocity model by adding ±0.7 km/s to model A (Fig. 2(a)). The bounding velocity range includes the true *P* velocity structure. In the reference models, only the *P*-wave velocities are defined. The *S*-velocity structures are obtained from the *P*-velocity structures using the V_P/V_S ratio.

Two additional velocity modes are considered to examine the dependence of inverted hypocentral parameters on the structure of velocity model (Fig. 2(b)). We design a velocity with half the number of layers in model A. The velocity model is constructed by merging two adjacent layers into a single layer. Another velocity model is designed to have twice the number of layers. The model is constructed by dividing each layer into two layers. The changes in numbers of layers naturally incorporate changes in thicknesses of layers.

We first verify the proposed method from synthetic experiments in ideal monitoring environment. We consider ten events (e1–e10) of epicenter S1 with different focal depths (Fig. 3). The epicenter S1 is located at 36.5°N and 127.0°E. The focal depths of the events are 2.3, 6.1, 10.8, 14.7, 19.4, 23.6, 27.5, 30.9, 43.2 and 54.6 km (Table 1). Twenty stations are distributed homogeneously around the epicenter with good azimuthal coverage (Table 3). The epicentral distances range between 4.2 and 117.7 km (Fig. 3). Synthetic traveltimes of first-arrival *P* and *S* phases at the stations are calculated for the ten events.

We also test the proposed method for hypocentral inversion in ill condition. Epicenter S2 and twelve stations at localized azimuths (filled triangles) are considered (see, Fig. 3). The epicenter S2 is located at 37.0°N and 126.9°E with the focal depth of 10.8 km. The azimuths of stations vary between 129.7° and 204.0°, and the epicentral distances are between 6.9 and 122.1 km. The synthetic traveltimes at the stations are calculated.

The efficiency of the proposed algorithm is tested using the arrival times of first-arrival phases considering practical application to field data in which particular phases are not identifiable in the initial stage. We analyze the first-arrival *P* and *S* phases, which can be easily picked in field data. The first-arrival *P* and *S* phases vary depending on the

Table 1
A velocity model with 9 layers for computation of synthetic arrival times. The focal depths of 10 events, *P* and *S* velocities (V_P, V_S), and V_P/V_S ratios are presented.

Layer	Depth (km)	V_p (km/s)	V_s (km/s)	V_P/V_S	Events (focal depth, km)
1	2.5	5.70	3.33	1.712	e1 (2.3)
2	6.7	5.90	3.41	1.730	e2 (6.1)
3	11.5	6.15	3.53	1.742	e3 (10.8)
4	16.4	5.95	3.39	1.755	e4 (14.7)
5	21.2	6.35	3.66	1.735	e5 (19.4)
6	26.6	6.50	3.79	1.715	e6 (23.6)
7	32.0	6.60	3.88	1.701	e7, e8 (27.5, 30.9)
8	50.0	8.00	4.61	1.735	e9 (43.2)
9	80.0	8.05	4.63	1.739	e10 (54.6)

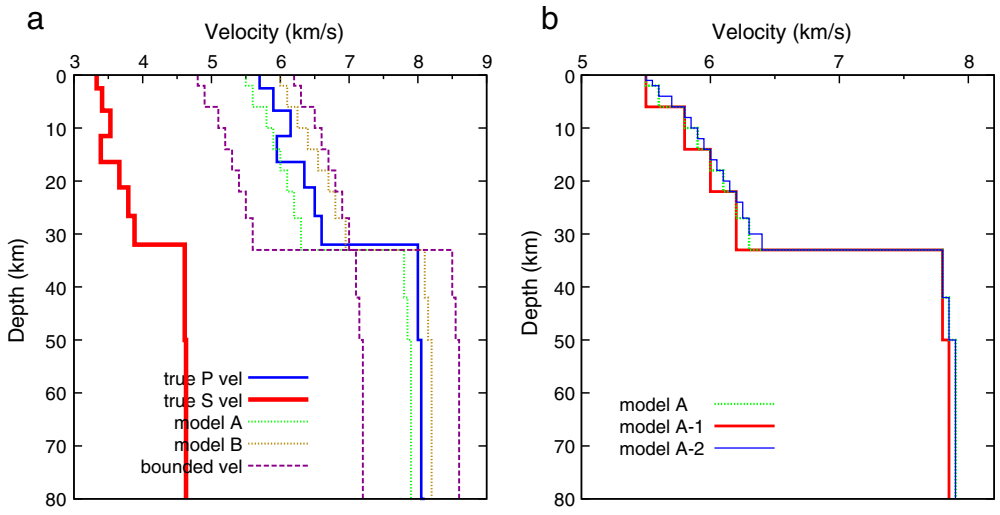

Fig. 2. (a) Velocity models implemented for inversion of hypocentral parameters. True *P* and *S* velocity structures are presented with solid lines (red and blue lines). Model A is composed of low *P* velocities, and model B consists of high *P* velocities. A bounded *P* velocity model is constructed for inversion with GA-MHYPO. Model A is used for the lower bound of velocity, and the upper bound of velocity is designed by adding ± 0.7 km/s to the lower bound of velocity. (b) *P* velocity models with different numbers of layers. Model A is used for the reference velocity model. Model A-1 has a half the number of layers, and model A-2 has the twice the number of layers compared to that of model A.

distance and velocity structure. For example, the Moho head waves (*Pn*, *Sn*) are the first-arrival phases at regional distances, whereas direct waves (*Pg*, *Sg*) are the first arrivals at local distances.

The reference arrival times in the true velocity model are calculated using a two-point ray tracing in which computational errors are as small as less than 10^{-10} s (Kim and Baag, 2002). We regard the calculated synthetic data as error-free. Noise-added data are then created by combining the noise-free data with random noise of 0.1 s standard deviation. The heterogeneities along raypaths cause fluctuations in traveltimes, and broaden the wavelets with loss of high frequency energy (e.g., Hong and Kennett, 2003; Hong et al., 2005; Müller and Shapiro, 2001; Sato, 1989). The influence of heterogeneities along raypaths causes errors in phase picking and measurement of traveltimes. These raypath effects increase with distance. Thus, we design random errors to increase with epicentral distance; large errors are assigned to the traveltimes for stations at large epicentral distances, and small errors are assigned to those for stations at short epicentral distances.

4. Inversion methods

Conventional methods are based on ray tracing for calculating traveltimes and raypaths between the source and receivers. Thus, the accuracy and convergence rate of ray tracing are crucial factors for accurate and efficient hypocentral inversion. Kim and Baag (2002) introduced a two-point ray tracing with high precision. The two-point ray tracing algorithm was found to be useful for determining traveltimes in local and regional distances through media with fine structures (Kim and Baag, 2002).

In this study, we test the accuracy of the proposed efficient inversion scheme with different inversion methods. Since the accuracy of the ray tracing algorithm is critical in the accuracy of the inverted hypocentral parameters, we examine methods that use the same ray tracing algorithm. We apply two methods representing two groups of inversion methods.

Table 2
Two adopted *P* velocity models (A, B) with 11 layers. The *P* velocities of model A are lower than those in the true model, whereas those of model B are larger.

Layer	Depth (km)	Model A V_p(km/s)	Model B V_p(km/s)
1	2	5.50	6.00
2	6	5.60	6.10
3	10	5.80	6.25
4	14	5.90	6.40
5	18	6.00	6.55
6	22	6.10	6.70
7	27	6.20	6.80
8	33	6.30	6.95
9	42	7.80	8.10
10	50	7.85	8.15
11	80	7.90	8.20

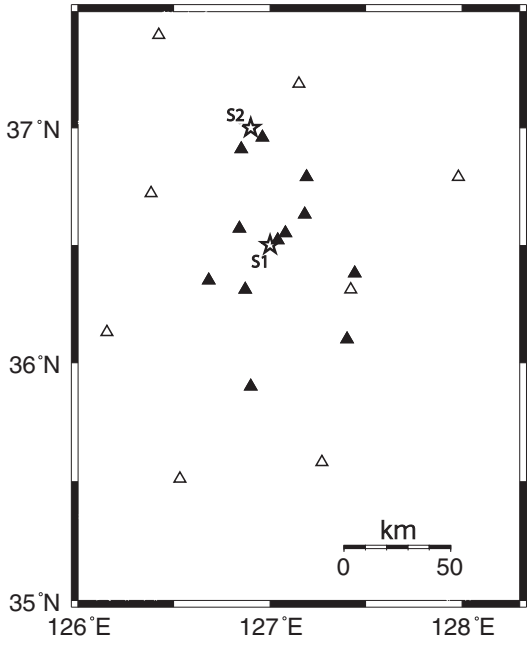

Fig. 3. Locations of 2 epicenters (stars) and 20 stations (triangles). Ten events with various focal depths are considered at the epicentral location of S1. All stations (open and filled triangles) are used for hypocentral inversions of events at epicenter S1. Twelve stations (filled triangles) are used for hypocentral inversion of event S2. Hypocentral inversion for event S2 is designed for a test of ill condition.

Table 3
Locations (latitude, longitude) of twenty stations (R01–R20) and their epicentral distances and azimuths to two epicenters (S1, S2). All stations are used for hypocentral inversion of epicenter S1, and 12 stations for hypocentral inversion of epicenter S2.

ID	Lat (°N)	Long (°E)	Event recorded	Dist (km)	Azi (°)
R01	36.52	127.04	S1, S2	4.22, 54.71	58.22, 166.75
R02	36.55	127.08	S1, S2	9.06, 52.46	52.22, 162.10
R03	36.57	126.84	S1, S2	16.30, 48.02	298.51, 186.42
R04	36.63	127.18	S1, S2	21.63, 48.06	48.11, 148.59
R05	36.31	126.87	S1, S2	24.09, 76.62	208.99, 182.01
R06	36.35	126.68	S1, S2	33.18, 74.76	239.98, 195.31
R07	36.79	127.19	S1, S2	36.39, 34.80	27.78, 131.94
R08	36.38	127.44	S1, S2	41.64, 84.04	108.52, 144.79
R09	36.91	126.85	S1, S2	47.43, 10.93	343.63, 204.04
R10	36.96	126.96	S1, S2	51.17, 6.94	356.01, 129.70
R11	36.10	127.40	S1, S2	57.11, 109.45	140.89, 155.70
R12	35.90	126.90	S1, S2	67.18, 122.06	187.72, 0.00
R13	36.72	126.38	S1	60.61	293.94
R14	37.19	127.15	S1	77.74	9.87
R15	36.13	126.15	S1	86.68	241.98
R16	36.79	127.98	S1	93.37	69.55
R17	37.31	127.42	S1	97.38	22.48
R18	35.58	127.27	S1	104.94	166.51
R19	37.40	126.42	S1	112.46	332.82
R20	35.51	126.53	S1	117.74	201.23

The accuracy of the inverted hypocentral parameters depends on the implemented velocity model. The adopted velocity model may differ from the actual structure, especially in the case of 1-D models. Simultaneous inversion of hypocentral parameters and velocity structures may be a useful approach for obtaining accurate results.

Conventional methods can be classified into two groups according to whether the velocity models are refined or not. One group of methods including HYPO71 (Lee and Lahr, 1975; Lee, 1990), HYPOINVERSE (Klein, 1978, 2002) and HYPOELLIPSE (Lahr, 1980, 1999) determines the hypocentral parameters based on given velocity models. The other group of methods including VELEST (Kissling et al., 1994) determines the hypocentral parameters along with the refinement of the velocity models.

In this study, we implement a hypocentral inversion method based on a two-point ray tracing method, MHYPO (Hahm et al., 2007), in which the inversion algorithm is modified from HYPO-71. The method introduces weighting factors reflecting the degree of confidence in focal depths from the hypocentral inversion. Here, MHYPO stands for the group of methods based on given velocity models.

We introduce GA-MHYPO (Kim et al., 2006) to stand for the group of methods determining the hypocentral parameters and velocity models. GA-MHYPO combines MHYPO with a genetic algorithm to refine the velocity models. The method retains high precision in hypocentral inversion, but requires large computational resources. GA-MHYPO searches for the best-fitting *P* and *S* velocities in each layer in the prescribed velocity ranges. The best-fitting velocities are searched using a fitness function that assesses the differences between the observed and theoretical traveltimes of *P* and *S* waves. The determined velocities of layers may not match the true velocities, but the estimated weighted average velocity between a source and stations should be close to the true weighted average velocity.

The efficient inversion algorithm proposed in this study is applicable to any conventional inversion method. We design an inversion method combining MHYPO with the algorithm, referred to as VELHYPO, to test the accuracy of the algorithm. VELHYPO searches for the best-fitting average velocity using a fitness function among a given set of velocity models. The best-fitting average velocity is refined through successive iterations. In principle, the number of effective decimal points of average velocity increases with the iteration. The refinement of average velocity continues until it converges.

5. Computational results

The accuracy of inverted hypocentral parameters is compared among three methods (MHYPO, VELHYPO, and GA-MHYPO). MHYPO and VELHYPO invert for hypocentral parameters with velocity models A and B and average V_P/V_S ratios. The velocity models are refined in VELHYPO, whereas fixed velocity models are used in MHYPO. GA-MHYPO implements a prescribed velocity range along with the average V_P/V_S ratio. The computational time of VELHYPO is about 100 times faster than that of GA-MHYPO, but about 50 times slower than that of MHYPO as result of the iterations to search for the best-fitting velocity model. The three methods are also applied to natural earthquake data, and the inverted hypocentral parameters are compared.

5.1. Test with synthetic noise-free data

Noise-free synthetic data are inverted for hypocentral parameters using the three methods (MHYPO, VELHYPO, GA-MHYPO; Fig. 4). The epicenter errors of MHYPO based on models A and B range between 0.17 and 0.74 km, and are much larger than those of the other methods (Fig. 4(a)). In contrast, epicenter errors of VELHYPO and GA-MHYPO are less than 0.02 km. This is because MHYPO inverts for the hypocentral parameters based on given velocity models, whereas VELHYPO and GA-MHYPO are based on refined velocity models. Thus, the accuracy of the inverted epicenters by MHYPO is highly dependent on the implemented velocity models. The epicenter errors of VELHYPO and GA-MHYPO, however, do not appear to vary much with the initial models.

The focal depth errors are comparable between VELHYPO and GA-MHYPO, and are less than 0.14 km (Fig. 4(b)). The focal depth errors of VELHYPO and GA-MHYPO are much lower than those of MHYPO. Notably, the focal depth errors of MHYPO appear to vary with the focal depth. The focal depth errors of MYHPO are determined to be 0.22–4.17 km for shallow six events (e1–e6), and are much smaller for deeper events (e7–e10). The focal depth errors are greater than the epicenter errors for all methods.

The MHYPO origin time errors are determined to be 0.38–0.61 s, which are significantly larger than those of VELHYPO and GA-MHYPO (Fig. 4(c)). VELHYPO and GA-MHYPO have small origin time errors of less than 0.04 s. These results indicate that the hypocentral parameters inverted from MHYPO based on velocity models A and B display much higher errors than those from VELHYPO and GA-MHYPO. Thus, the accuracy of the implemented velocity models appears to be critical for accurate inversion of hypocentral parameters in inversion methods based on the given velocity models.

In VELHYPO and GA-MHYPO, the errors for events in the lower crust (e6–e8) are similar to those for other events. The first-arrival phases of lower-crustal events are the Moho head waves at long-distance stations (e.g., stations R14-R20 for event e7). In contrast, the upper-mantle events (e9 and e10) do not produce the Moho head waves, and direct waves are the first-arrival phases. Thus, the arrival-time inversions based on the composite set of the Moho head waves and direct waves are performed well.

Typically, different velocity models are obtained for each event from inversions with VELHYPO and GA-MHYPO. Fig. 5 presents an example of inverted velocity models for event e10 with a focal depth of 54.6 km. The velocity models inverted from VELHPYPO and GA-MHYPO do not match the true model, but do vary around the true model. In addition, the low velocity zone in the true velocity model is not resolved in the inverted velocity models from VELHYPO and GA-MHYPO.

The weighted average *P* velocities are determined to be 6.72 km/s for MHYPO with model A, 7.17 km/s for MHYPO with model B, 6.96 km/s for VELHYPO with initial model A, 6.97 km/s for VELHYPO with initial model B and 6.95 km/s for GA-MHYPO. Here, the true average *P* velocity is 6.96 km/s. The average velocities are close to the true value in inversions with VELHYPO and GA-MHYPO. However, since the velocity models are

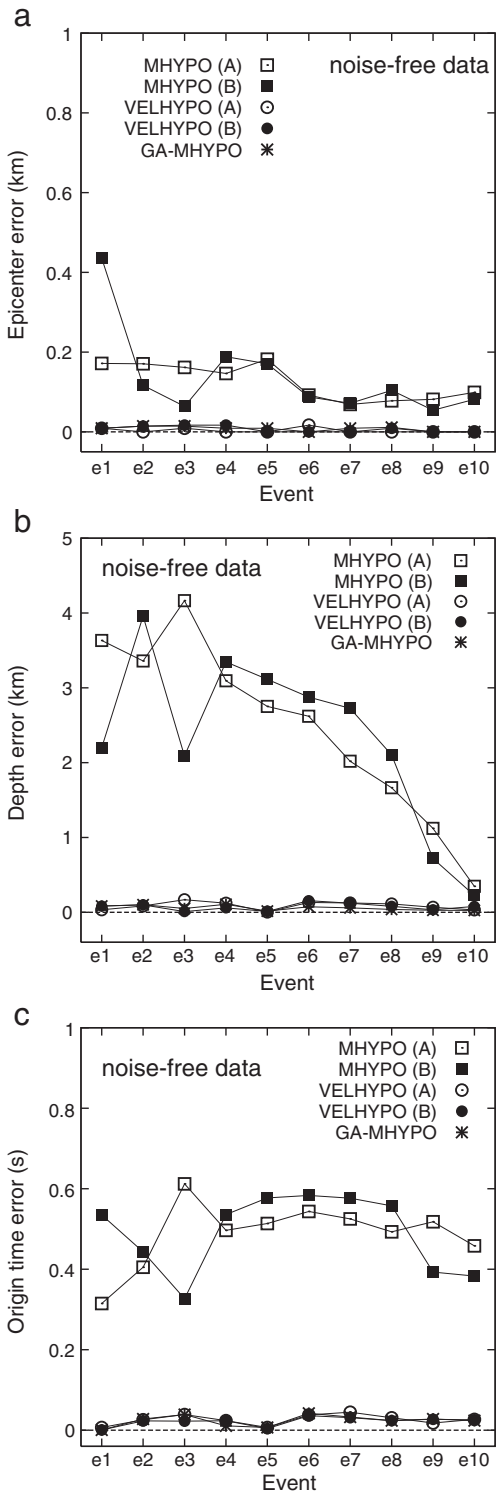

Fig. 4. Comparison of errors in inverted hypocentral parameters for noise-free data of various methods: (a) epicentral locations, (b) focal depths, and (c) origin times. MHYPO has higher errors than VELHYPO and GA-MHYPO for all hypocentral parameters.

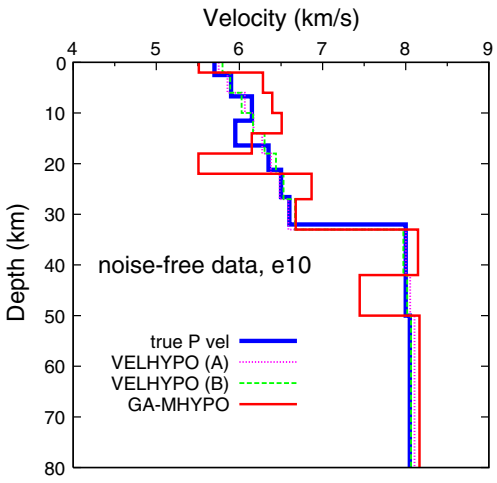

Fig. 5. Comparison of *P* velocity models inverted from noise-free data of event e10 among the methods. The average velocities of inverted velocity models are close to the average velocity of the true model.

not refined in MHYPO, the average velocities are different from the true value.

5.2. Test with synthetic noise-added data

Now we test the accuracy of the proposed algorithm for noise-added synthetic data (Fig. 6). The general trends in errors of hypocentral parameters are similar to those observed in noise-free data. Epicenter errors from inversions with noise-added data are five or more times higher than those from inversions with noise-free data. The epicenter errors of MHYPO are larger than those of other methods. The epicenter errors of MHYPO are 0.06–0.33 km for most events. On the other hand, the epicenter errors are determined to be similar between VELHYPO and GA-MHYPO, with values of less than 0.23 km.

The focal depth errors of MHYPO present similar trends between models A and B. The focal depth errors of MHYPO range between 1.4 and 2.6 km for most events. The focal depth errors of MHYPO are much larger than the errors of less than 0.30 km, found for VELHYPO and GA-MHYPO. The origin time errors of MHYPO are similar between models A and B, and range between 0.28 and 0.59. VELHYPO and GA-MHYPO have origin time errors less than 0.18 s, which are lower than those of MHYPO.

An example of the inverted velocity models for event e10 with a focal depth of 54.6 km is presented in Fig. 7. The inverted velocity models of VELHYPO are similar to those for noise-free data (cf., Fig. 5). In contrast, the inverted velocity models of GA-MHYPO are much different from those for noise-free data because GA-MHYPO searches for a velocity model that minimizes the error of a given noise-added data set by adjusting the velocity in each layer. On the other hand, VELHYPO searches for a velocity model yielding the minimum error by shifting the given velocity structure by a constant amount.

The weighted average *P* velocities are 6.97 km/s for VELHYPO based on model A, 6.98 km/s for VELHYPO based on model B, and 6.98 km/s for GA-MHYPO. Here the true weighted average *P* velocity is 6.96 km/s. The inverted weighted average velocities are similar between VELHYPO and GA-MHYPO. The resultant origin time errors are comparable between VELHYPO and GA-MHYPO. Inversions based on weighted average velocities (VELHYPO) appear to yield sufficiently accurate results even for noise-added data, and the computational times are much reduced compared to full-velocity inversion methods (e.g., GA-MHYPO).

Note that the inverted velocity models are not similar between VELHYPO and GA-MHYPO although the errors in hypocentral parameters are comparable. In particular, GA-MHYPO has a high degree of freedom in inversion, and does not yield a velocity model envisaging the true velocity structure because the inverted model is determined to have the minimum error for the given data. This observation suggests that prior information constraining the velocity structures

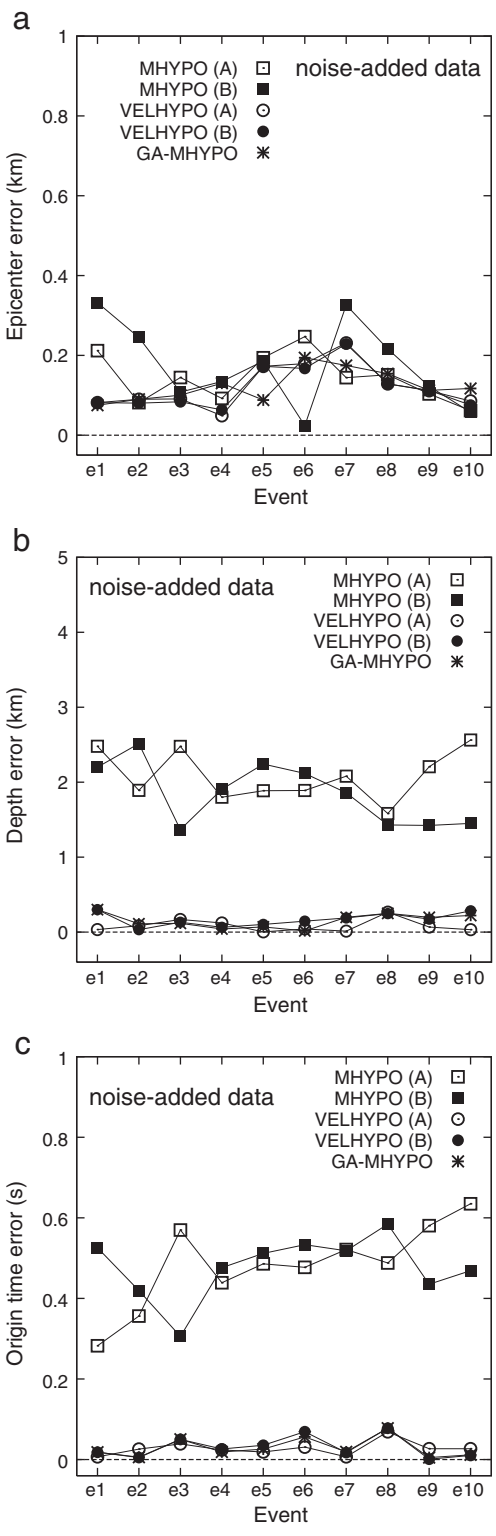

Fig. 6. Comparisons of errors in the inverted hypocentral parameters for noise-added data among methods: (a) epicentral locations, (b) focal depths, and (c) origin times. The errors from MHYPO are higher than those from VELHYPO and GA-MHYPO. The errors in epicentral locations and origin times are larger than those of noise-free data.

may be needed for accurate velocity inversion. In this study, the overall errors of hypocentral parameters are larger for noise-added data than for noise-free data.

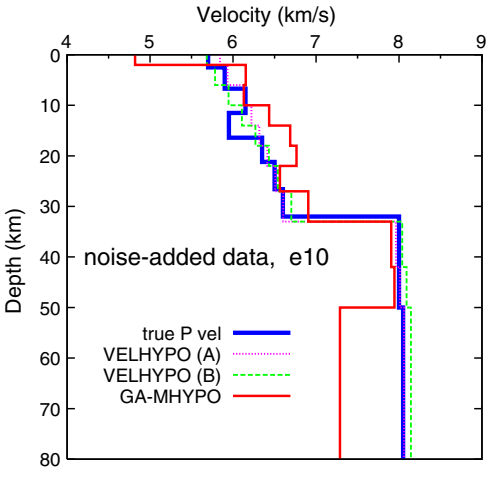

Fig. 7. Comparison of inverted *P* velocity models for noise-added data of event e10. The average velocities of inverted velocity models are similar to the average velocity of the true model.

5.3. Tests for ill condition and velocity-model dependence

Hypocentral inversion in ill condition is challenging for every inversion method. We perform a hypocentral inversion of event S2 using traveltimes at twelve stations in localized azimuths (Fig. 3). The inverted hypocentral parameters are presented in Table 4. Both VELHYPO and GA-MHYPO determine the hypocentral parameters reasonably well, while MHYPO yields relatively poor results. Note that VELHYPO and GA-MHYPO update the velocity model in every iteration during hypocentral inversion, while MHYPO is performed using a fixed velocity model. In particular, VELHYPO that incorporates the algorithm proposed in this study determine both the hypocentral location and the origin times well. The observation suggests that the method proposed in this study works reasonably even in ill condition.

We additionally test the influence of the number of layers in velocity model on the accuracy of inverted hypocentral parameters. Model A is used for a reference velocity model. Model A-1 is composed of a half the layers compared to model A, and model A-2 consists of twice the layers (Fig. 2(b)). The hypocentral inversions are performed based on VELHYPO. The errors in hypocentral parameters are comparable among velocity models with different numbers of layers (Fig. 8). The observation suggests that the inverted hypocentral parameters are rarely dependent on the structure of velocity model as long as a sufficient number of layers is implemented.

5.4. Natural earthquake data

We apply the inversion methods to three natural earthquakes that occurred in the Korean Peninsula. We analyze 14 arrival-time data from the 26 April 2004 earthquake of M_L 4.0 (Seongju earthquake), 15 data from the 20 January 2007 earthquake of M_L 4.9 (Odaesan earthquake), and 19 data from the 1 May 2009 event of M_L 3.9 (Andong earthquake; Table 5). The hypocentral parameters of the earthquakes are determined by three representative methods (MHYPO, GA-MHYPO,

Table 4
True and inverted hypocentral parameters of event S2. Hypocentral inversions are performed based on model A in Table 2.

Method	Origin time difference (s)	Lat (°N)	Long (°E)	Depth (km)	P-RMS error (s)
True value	0	37.0000	126.9000	10.800	–
MHYPO	−0.972	36.9763	126.9063	12.188	0.132
VELHYPO	0.003	36.9975	126.9011	10.926	0.005
GA-MHYPO	−0.003	36.9988	126.9005	10.952	0.004

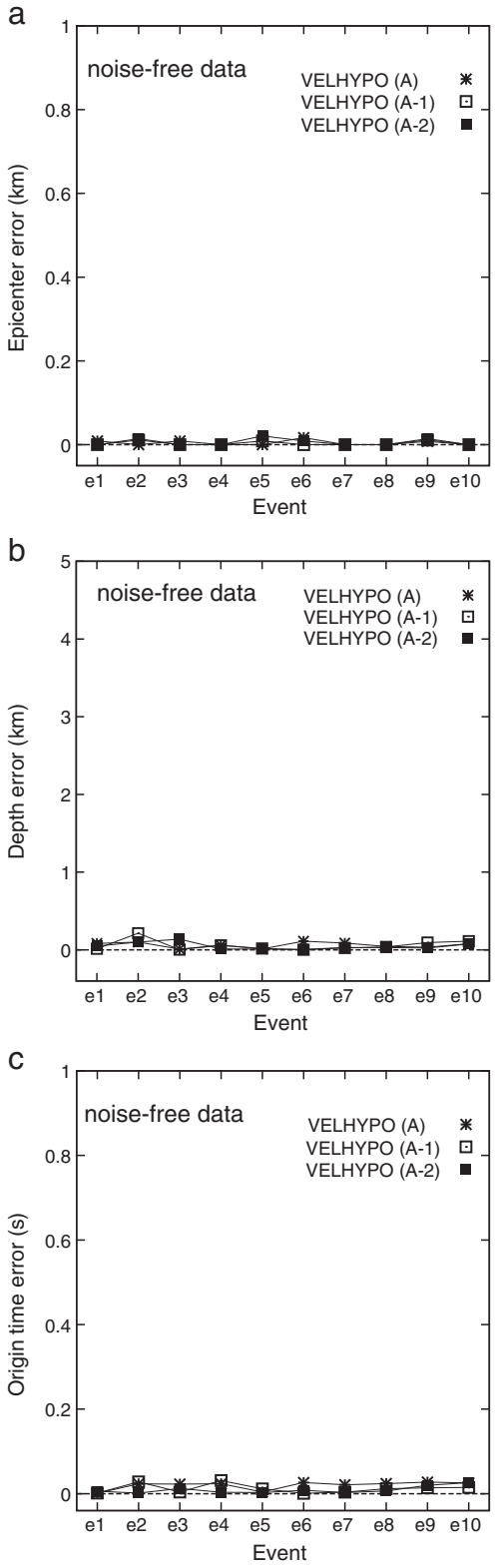

Fig. 8. Comparison of errors in inverted hypocentral parameters for velocity models with different numbers of layers: (a) epicentral locations, (b) focal depths, and (c) origin times. Model A-1 has a half the number of layers of model A, and model A-2 has the twice the number of layers of model A. The hypocentral inversions are performed based on VELHYPO.

and VELHYPO). Note that MHYPO implements a fixed velocity model for hypocentral inversion. Thus, the accuracy of inverted hypocentral parameters is expected to be highly dependent on the accuracy of implemented velocity models. On the other hand, GA-MHYPO and VELHYPO update the velocity models in the inversion process, and determine hypocentral parameters for optimum velocity models.

The inverted hypocentral parameters are compared among the three methods in Table 5. The root-mean-square errors in *P* arrival times (*P*-RMS) of the three events are less than 0.06 s for VELHYPO and GA-MHYPO, but 0.10–0.18 for MHYPO. The hypocentral parameters are also very similar between VELHYPO and GA-MHYPO for each event (Fig. 9). The differences in origin times, epicenters, and focal depths between VELHYPO and GA-MHYPO are less than 0.15 s, 0.5 km and 0.5 km, respectively, which are similar to those observed in the synthetic data analysis. MHYPO, however, produces hypocentral parameters that deviate from those of VELHYPO and GA-MHYPO. The consistent determination of hypocentral parameters between VELHYPO and GA-MHYPO suggests that VELHYPO is more efficient than GA-MHYPO for inversions of hypocentral parameters.

6. Implementation in a conventional method

This section examines the transportability of the proposed algorithm to a conventional method. The algorithm is implemented in HYPOELLIPSE (Lahr, 1980). We examine the improvement in computational accuracy. The combination of HYPOELLIPSE with the proposed algorithm is referred to herein as VELELLIPSE. The proposed algorithm iteratively searches for the best-fitting average velocity. Thus, VELELLIPSE performs iterative inversions based on refined average velocities, whereas HYPOELLIPSE conducts a single inversion based on a given velocity model. The velocity models in the synthetic tests are used (Table 2, Fig. 2).

We invert for hypocentral parameters with VELELLIPSE and HYPOELLIPSE using the noise-free and noise-added synthetic data applied in the previous synthetic tests. Fig. 10 compares the errors of the inverted hypocentral parameters between the methods. In inversions with noise-free data, the errors of hypocentral parameters from VELELLIPSE are much smaller than those from HYPOELLIPSE (Fig. 10(a),(b),(c)). The overall features of errors are similar to those observed between MHYPO and VELHYPO (see Fig. 4).

Considering the typical errors in phase picking and traveltime fluctuations in local distances, random noises with a standard deviation of 0.1 s are generated. The random noises are added to the noise-free synthetic traveltimes. Here, we allocate large noises (or, errors) to traveltimes for stations in long distances, and small noises (or, errors) to traveltimes for station in short distances considering the usual raypath effects that increase with distance. HYPOELLIPSE and VELELLIPSE are applied for hypocentral inversion with the noise-added traveltime data. It is observed that the epicenter errors are comparable between HYPOELLIPSE and VELELLIPSE (Fig. 10(d)). Note that the epicenter errors of VELHYPO are much smaller than those of MHYPO for the same noise-added data

Table 5
Comparison between the reported and inverted hypocentral parameters of three natural earthquakes. The reported source parameters are collected from the Korea Institute of Geoscience and Mineral Resources (KIGAM) bulletin.

Event	Method	Origin time	Lat (°N)	Long (°E)	Depth (km)	P-RMS (s)
	Reported	04:29:25.4	35.8248	128.2391	8.1	–
2004/04/26	MHYPO	04:29:25.3361	35.8353	128.2339	16.2679	0.1023
(M_L4.0)	VELHYPO	04:29:25.8176	35.8381	128.2307	12.3699	0.0434
	GA-MHYPO	04:29:25.9730	35.8378	128.2304	12.2573	0.0423
	Reported	11:56:53.6	37.6889	128.5841	13.1	–
2007/01/20	MHYPO	11:56:53.1567	37.6693	128.5829	11.0979	0.1801
(M_L4.9)	VELHYPO	11:56:53.6152	37.6867	128.5922	9.4653	0.0358
	GA-MHYPO	11:56:53.6778	37.6875	128.5928	8.9933	0.0388
	Reported	22:58:27.99	36.5556	128.7120	11.4	–
2009/05/01	MHYPO	22:58:27.8598	36.5566	128.7032	14.6402	0.1090
(M_L3.9)	VELHYPO	22:58:28.5124	36.5572	128.7101	9.7983	0.0508
	GA-MHYPO	22:58:28.5023	36.5587	128.7097	9.6902	0.0588

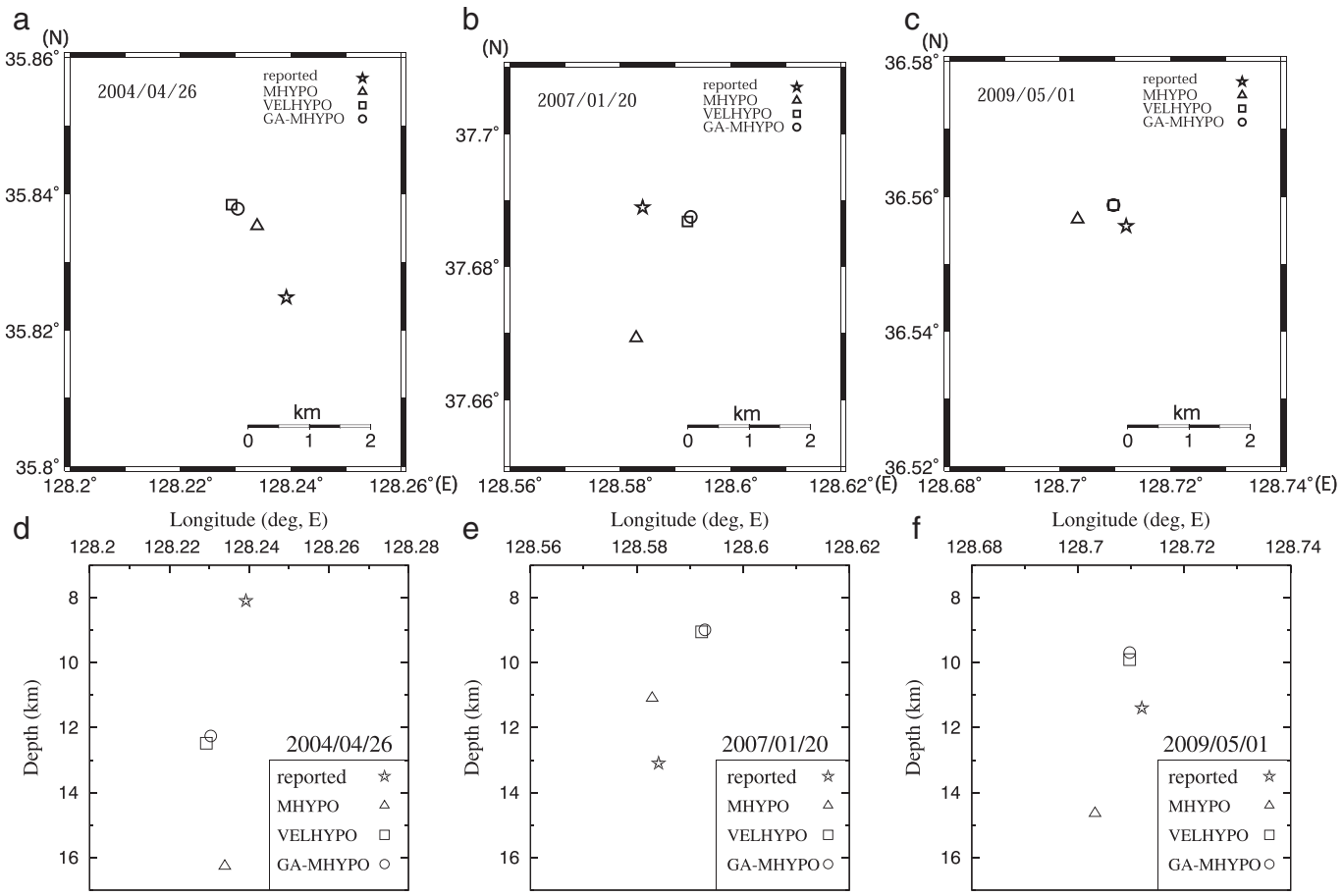

Fig. 9. Epicenters (upper figures) and depths (lower figures) of three natural earthquakes: (a) and (d) are for the 26 April 2004 M_L 4.0 earthquake, (b) and (e) are for the 20 January 2007 M_L 4.9 earthquake, and (c) and (f) are for the 1 May 2009 M_L 3.9 earthquake. The reported epicentral locations are marked with stars. The determined locations are marked with triangles (MHYPO), squares (VELHYPO) and circles (GA-MHYPO). The hypocenters determined by GA-MHYPO and VELHYPO are similar and highly accurate.

(Fig. 6(a)). However, the accuracy of origin times and depths are greatly improved in VELELLIPSE (Fig. 10(e),(f)).

The comparisons between hypocentral parameters suggest that the proposed algorithm does not lead to much improvement in epicenter accuracy when error-included arrival times are applied in inversions based on HYPOELLIPSE. In addition, in epicenter determination using HYPOELLIPSE, the arrival-time picking errors may be more significant in inversions than the errors in the velocity models. These features appear to be associated with the accuracy of the ray tracing adopted in inversion methods. The inherent accuracy limitation of inversion methods may induce errors that are much higher than those improved by velocity-model refinement.

7. Conclusions

We have presented an inversion algorithm based on arbitrary 1-D velocity models for inversion of hypocentral parameters. The 1-D velocity models are constrained by the average velocities and velocity gradients of the media. The accuracy of the proposed algorithm was tested using three methods (MHYPO, VELHYPO, GA-MHYPO) for synthetic and field data. Only the *P*-wave velocity models are required in the algorithm. The *S*-wave velocities are inferred using the mean V_P/V_S ratios obtained from the observed traveltime differences between *P* and *S* waves.

Our results indicate that the inversion method based on weighted average velocities and velocity gradients yields accurate parameters at low computational costs compared to the usual full inversion methods. The computational time of VELHYPO is about 70 times lower than that of GA-MHYPO. Also, the errors in inverted hypocentral parameters are found to be small, which is difficult to achieve in conventional methods based on fixed velocity models. In particular, the proposed scheme particularly improves the accuracy of focal depths and origin times. The proposed algorithm was tested for hypocentral inversions with synthetic and field data. It was observed that the proposed algorithm works well even for inversion in ill condition in which stations are placed in localized azimuths. In addition, the proposed scheme is found to be rarely dependent on the structure of velocity model for accurate hypocentral inversion.

We analyzed first-arrival phase data, which may include head waves and direct waves in regional distances. The degree of combination between head waves and direct waves is dependent on the epicentral distances and focal depth in a data set. The proposed algorithm is applicable to any data set with both head waves and direct waves, and can be implemented with any form of velocity model that satisfies the average velocities and velocity gradients of the actual structures. In this study, inversions based on different forms of velocity models with the same average velocities and velocity gradient produced similar hypocentral parameters. It was demonstrated that the proposed scheme is simple and computationally efficient. The scheme can also be readily implemented in any conventional method.

It is noteworthy that the degree of accuracy improvement in inverted hypocentral parameters by implementation of the proposed scheme can differ according to the inversion method because every inversion method has its inherent accuracy limit. The accuracy of the ray tracing algorithm

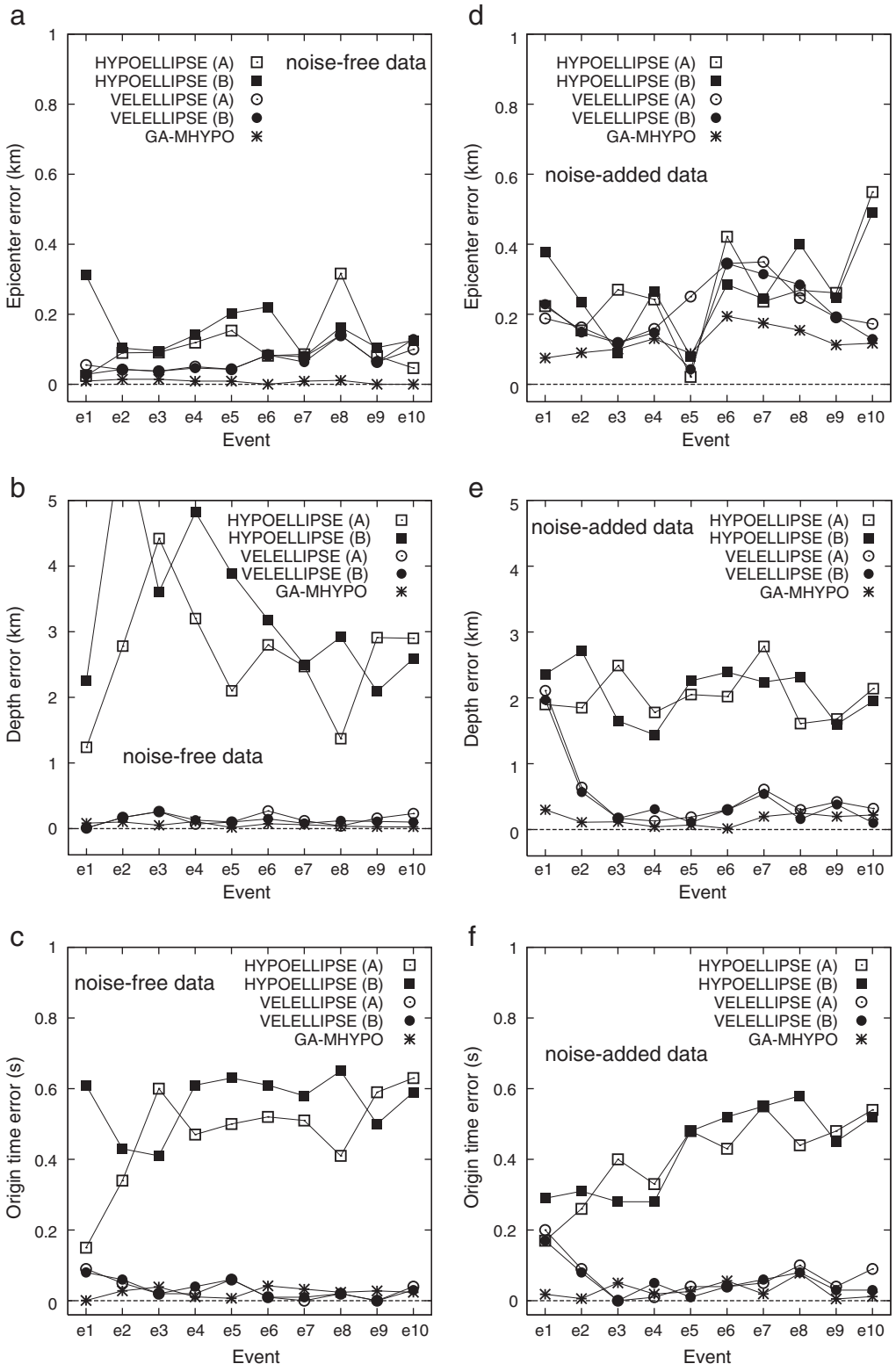

Fig. 10. Comparisons of the errors in inverted hypocentral parameters between HYPOELLIPSE and VELELLIPSE. The errors of GA-MHYPO are also presented for reference. Results for noise-free data (a,b,c) and noise-added data (d,e,f) are presented. The upper figures (a,d) present the errors in epicentral locations, the middle figures (b,e) show the errors in focal depths, and the lower figures (c,f) are the errors in the origin times. Significant accuracy improvement is observed in depth and origin time with implementation of the proposed algorithm in a conventional method. The epicenter errors are similar between HYPOELLIPSE and VELELLIPSE.

adopted in the inversion method is particularly important for improving the accuracy in the inverted hypocentral parameters. The proposed algorithm is expected to be especially useful for regions in which the velocity structures are poorly known or highly complex.

Acknowledgments

Some figures are generated using GMT (Wessel and Smith, 1998). We are grateful to the guest editor Professor José Badal, and two

anonymous reviewers for fruitful review comments. This work was funded by the Korea Meteorological Administration Research and Development Program under Grant CATER 2012-8130.

References

Asch, G., Wylegalla, K., Hellweg, M., Seidl, D., Rademacher, H., 1996. Observations of rapid-fire event tremor at Lascar volcano, Chile. Annals of Geophysics 39 (2), 273–282.

Bolt, B.A., 1960. The revision of earthquake epicenters, focal depths, and origin times using a high-speed computer. Geophysical Journal of the Royal Astronomical Society 3, 433–440.

Chiarabba, C., Frepoli, A., 1997. Minimum 1D velocity models in Central and Southern Italy: a contribution to better constrain hypocentral determinations. Annals of Geophysics 40 (4), 937–954.

Delibasis, N., Ziazia, M., Voulgaris, N., Papadopoulos, T., Stavrakakis, G., Papanastassiou, D., Drakatos, G., 1999. Microseismic activity and seismotectonics of Heraklion Area (central Crete Island, Greece). Tectonophysics 308 (1–2), 237–248.

Douglas, A., 1967. Joint epicenter determination. Nature 215, 47–48.

Engdahl, E.R., Gunst, R.H., 1966. Use of a high speed computer for preliminary determination of earthquake hypocenters. Bulletin of the Seismological Society of America 56, 325–336.

Fäh, D., Kind, F., Giardini, D., 2001. A theoretical investigation of average H/V ratios. Geophysical Journal International 145, 535–549.

Flinn, E.A., 1965. Confidence regions and error determinations for seismic event location. Reviews of Geophysics 3, 157–185.

Gambino, S.P., Mostaccio, A., Patané, D., Scarfi, L., Ursino, A., 2004. High-precision locations of the microseismicity preceding the 2002–2003 Mt. Etna eruption. Geophysical Research Letters 31. http://dx.doi.org/10.1029/2004GL020499.

Geiger, L., 1912. Probability method for the determination of earthquake epicenters from the arrival time only. Bulletin of the Saint Louis University 8, 60–71.

Hahm, I.K., Kim, W., Lee, J.M., Jeon, J.S., 2007. Determination of hypocentral parameters of local earthquakes using weighting factor based on take-off angle. Geosciences Journal 11, 39–49.

Hong, T.-K., Kennett, B.L.N., 2003. Scattering attenuation of 2-D elastic waves: theory and numerical modeling using a wavelet-based method. Bulletin of the Seismological Society of America 93 (2), 922–938.

Hong, T.-K., Wu, R.-S., Kennett, B.L.N., 2005. Stochastic features of scattering. Physics of the Earth and Planetary Interiors 148, 131–148.

Husen, S., Kissling, E., Flueh, E., Asch, G., 1999. Accurate hypocentre determination in the seismogenic zone of the subducting Nazca Plate in northern Chile using a combined on-/offshore network. Geophysical Journal International 138 (3), 687–701.

Ito, A., Sugioka, H., Suetsugu, D., Shiobara, H., Kanazawa, T., Fukao, Y., 2012. Detection of small earthquakes along the Pacific–Antarctic Ridge from T-wave recorded abyssal ocean-bottom observatories. Marine Geophysical Researches 33. http://dx.doi.org/10.1007/s11001-012-9158-0.

Kim, W., Baag, C.-E., 2002. Rapid and accurate two-point ray tracing based on a quadratic equation of takeoff angle in layer media with constant or linearly varying velocity functions. Bulletin of the Seismological Society of America 92, 2251–2263.

Kim, W., Hahm, I.-K., Ahn, S.J., Lim, D.H., 2006. Determining the hypocentral parameters for local earthquakes in 1-D using genetic algorithms. Geophysical Journal International 166, 590–600.

Kissling, E., Ellsworth, W.L., Eberhart-Phillips, D., Kradolfer, U., 1994. Initial reference models in local earthquake tomography. Journal of Geophysical Research 99, 19635–19646.

Klein, F.W., 1978. Hypocenter Location Program HYPOINVERSE, US Geological Survey Open-File Report, 78-694. Menlo Park, CA.

Klein, F.W., 2002. Users Guide to HYPOINVERSE-2000, a Fortran Program to Solve for Earthquake Locations and Magnitudes. US Geological Survey Open-File Report, 02-171. Menlo Park, CA (123 pp.).

Lahr, J.C., 1980. HYPOELLIPSE/MULTICS: A Computer Program for Determining Local Earthquake Hypocentral Parameters, Magnitude, and First Motion Pattern, US Geological Survey Open-File Report, 59-80. Denver, CO.

Lahr, J.C., 1999. HYPOELLIPSE: a computer program for determining local earthquake hypocentral parameters, magnitude, and first-motion pattern (Y2K compliant version). US Geological Survey Open-File Report 99-23, Denver, CO.

Lee, W.H.K., 1990. Replace the HYPO71 format? Bulletin of the Seismological Society of America 80, 1046–1047.

Lee, W.H.K., Lahr, J.C., 1975. HYPO71 (Revised): A Computer Program for Determining Local Earthquake Hypocenter, Magnitude, and First Motion Pattern of Local Earthquakes. US Geological Survey Open-File Report, 75-311. Melon Park, CA (113 pp.).

Lin, G., Shearer, P.M., Hauksson, E., 2007. Applying a three-dimensional velocity model, waveform cross correlation, and cluster analysis to locate southern California seismicity from 1981 to 2005. Journal of Geophysical Research 112 (B12). http://dx.doi.org/10.1029/2007JB004986 B12309.

Magistrale, H., Jones, L., Kanamori, H., 1989. The Saperstition Hills, California, Earthquakes of 24 November 1987. Bulletin of the Seismological Society of America 79, 239–251.

Müller, T.M., Shapiro, S.A., 2001. Most probable seismic pulses in single realizations of two- and three-dimensional random media. Geophysical Journal International 144, 83–95.

Pavlis, G.L., Booker, J.R., 1983. A study of the importance on nonlinearity in the inversion of earthquake arrival time data for velocity structure. Journal of Geophysical Research 88, 5047–5055.

Prejean, S.G., Hill, D.P., Brodsky, E.E., Hough, S.E., Johnston, M.J.S., Malone, S.D., Oppenheimer, D.H., Pitt, A.M., Richards-Dinger, K.B., 2004. Remotely triggered seismicity on the United States west coast following the Mw 7.9. Denali fault earthquake Bulletin of the Seismological Society of America 94 (6), S348–S359.

Pujol, J., 1988. Comments on the joint determination of hypocenters and station corrections. Bulletin of the Seismological Society of America 78, 1179–1189.

Sato, H., 1989. Broadening of seismogram envelopes in the randomly inhomogeneous lithosphere based on the parabolic approximation: southeastern Honshu, Japan. Journal of Geophysical Research 94 (B12), 17,735–17,747.

Schweitzer, J., 1997. HYPOSAT—a new routine to locate seismic events. NORSAR Scientific Report 1–97 (98), 94–102.

Schweitzer, J., 2001. HYPOSAT—an enhanced routine to locate seismic events. Pure and Applied Geophysics 158, 277–289.

Thurber, C.H., 1985. Nonlinear earthquake location: theory and examples. Bulletin of the Seismological Society of America 75, 779–790.

Thurber, C.H., 1992. Hypocenter-velocity structure coupling in local earthquake tomography. Physics of the Earth and Planetary Interiors 75, 55–62.

Waldhauser, F., 2001. hypoDD: A Computer Program to Compute Double-Difference Earthquake Locations. US Geological Survey Open-File Report, 01-113. Menlo Park, CA.

Waldhauser, F., Ellsworth, W.L., 2000. A double-difference earthquake location algorithm: method and application to the Northern Hayward Fault. California, Bulletin of the Seismological Society of America 90, 1353–1368.

Waldhauser, F., Schaff, D.P., 2008. Large-scale relocation of two decades of Northern California seismicity using cross-correlation and double-difference methods. Journal of Geophysical Research 113. http://dx.doi.org/10.1029/2007JB005479 (B08311).

Wessel, P., Smith, W.H.F., 1998. New, improved version of generic mapping tools released, Eos Transactions. American Geophysical Union 79 (47), 579.